Scientific Journal of Impact Factor (SJIF): 4.72

e-ISSN : 2348-4470
p-ISSN : 2348-6406

International Journal of Advance Engineering and Research Development

National Conference On Nanomaterials, (NCN-2017)

Volume 4, Special Issue 6, Dec.-2017 (UGC Approved)

Hydrothermal Synthesis of Perovskite Oxides $CaMnO_3$ and $SrMnO_3$

S. Berbeth Mary[1], D.Edward Christy[2], S. Selvakumari[1], A. Leo Rajesh[1*]

[1]Department of Physics, St.Joseph's College (Autonomous), Tiruchirappalli-620 002, Tamil Nadu, India.
[2] Research Scholar, Research and Development Cenre, Bharathiyar University, Coimbatore – 641046, Tamil Nadu, India.

Abstract:-*Calcium Manganite ($CaMnO_3$) and Strontium Manganite ($SrMnO_3$) nanostructured perovskite oxides were prepared by cost effective and size controllable hydrothermal method at pH 9.2 with and without chelating agent. The as-prepared samples were annealed under air at 800°C. Single phase and crystalline material was observed by X-Ray diffraction and the average crystallite size was in the range of 40-60 nm. SEM Micrograph showed the homogeneously dispersed nanomaterials without agglomeration. Strong doublet peak around 550 cm^{-1} confirmed the formation of perovskite oxides by Fourier Transform Infrared Spectroscopy. The absorption peaks were observed by using UV- Visible spectroscopy and the band gap was estimated from Tauc's relation. The indirect band gap increased for the chelating agent used sample where it influenced by the crystallite size of the nanomaterials.*

Key words*: chelating agent, hydrothermal method, perovskite oxide, indirect band gap*

1. Introduction

Perovskite type oxide materials (ABO_3 where A is larger cation and B is a smaller cation) have received much attention due to their interesting electrical, electrochemical, superconducting, magnetic and thermoelectric properties [1-4]. These exceptional properties make them potential candidates in various novel electronic devices for energy storage applications. The development of environmental friendly and cost effective power sources overcomes the problems of energy crises and global warming. Thermoelectric power generation is a promising method of converting waste heat directly into electricity without any greenhouse gas emission. The efficiency of this thermoelectric material is determined by the figure of merit ZT. Dimensionless figure of merit is directly proportional to Seebeck coefficient (S), electrical conductivity (σ) and inversely proportional to thermal conductivity (κ) and absolute temperature (T). Good thermoelectric materials should have a large Seebeck coefficient, high electrical conductivity and low thermal conductivity where large electrical conductivity minimizes joule heating while low thermal conductivity maintains a temperature gradient between the hot and cold sides in the thermoelectric device. The intermetallic materials such as Bi_2Te_3 and $CoSb_3$ have a high ZT at low temperatures. However, they are toxic, rare and degrade at high temperatures under air [5]. Besides, thermoelectric materials are required to be stable at higher temperatures. Oxides are one of the best candidate materials for this requirement, but most oxides with high stability at high temperature in air are unsuitable for thermoelectric applications due to high electrical resistivity. These limitations were over welcomed by the discovery of Na_xCoO_2 with a high Seebeck coefficient (100MV/K at 300 K) and a low electrical resistivity (0.2 mΩ at 300K) by Terasaki et al in 1997 [6]. Due to its chemical, thermal stability and oxidation resistance in the air, $CaMnO_3$ (CMO) and $SrMnO_3$ (SMO) compounds are stable at higher temperatures [7].

Energy efficiency, environmentally friendly, recycling of unused components, high purity products, access of metastable and new phases, control of crystal size, morphology, composition, and polymorphism of the synthesized phases are the recompenses of hydrothermal method in synthesizing metal oxide nanocrystals. Experimental parameters such as temperature and pressure, pH, oxidation-reduction potential, concentration of chemical species, and the use of inorganic additives for homogeneous and heterogeneous nucleation can also be carefully controlled [8-10]. Homogeneous distribution of metal ions, reduced segregation, reduction of external temperature to form the required phase and large surface area were obtained when citric acid used as chelating agent [11 -13]. In this work CMO and SMO nanomaterials were prepared by hydrothermal method. The structural, morphological, functional and optical properties were analyzed.

2. Materials and Methods

AR Grade Calcium Nitrate tetra hydrate, Strontium Nitrate, Manganese (II) Nitrate hydrate, Citric acid anhydrous and Ammonia Solution (28%) were used without any further purification. CMO and SMO nanocrystals were prepared by hydrothermal method. Stoichiometric amounts of nitrates of calcium, strontium, manganese and equivalent amount of citric acid were dissolved in deionized water so that the metal ions can be consistently complexed together. Ammonia solution was added drop wise to the above mixed solution in which part of ammonia used to neutralize the unreacted citric acid. A sol was obtained when the pH value of the solution reached 9.2, then this sol was transferred to a 150 ml autoclave and the autoclave was placed into an oven for hydrothermal treatment at 200 °C for 20 h. The obtained precursors were centrifuged, washed with deionized water and ethanol for many times in order to remove the byproducts and dried at 120 °C overnight. The dried powders were calcined in air in a furnace at 800 °C for 4 h [14].

Crystal structure and phase purity were determined by Powder X-ray diffraction (XRD) and data were collected using a X-ray diffractometer (D8 Advanced) with Cu Kα radiation with a step up of 0.02° (λ=0.15406 nm). The surface morphology was observed by Scanning electron microscopy (SEM) with low and high magnifications. Fourier transform infrared (FTIR) spectra of the powder samples were recorded from 4000 to 400 cm^{-1} using a Perkin Elmer Fourier transform infrared spectrometer. The optical properties and the band gap were determined by using a Lambda 35 UV-Vis spectrometer.

3. Results and Discussion

Starting from the yellowish of the manganese nitrate solution, the suspension was bluish when pH reached 9.2. After hydrothermal treatment the powder became darkish due to the presence of different manganese valence states [15]. The XRD pattern of CMO and SMO nanomaterials prepared by hydrothermal method (a) by using a chelating agent (b) without chelating agent is shown in Fig. 1. Low crystalline powders were obtained for precursor whereas crystalline peaks were acquired from citric acid used sample. The results showed that the high quality crystalline and fine powders were achieved for the sample prepared with citric acid as chelating agent [16]. They clearly prove the single phase of the orthorhombic pervoskite structure of $CaMnO_3$ with JCPDS Card no 46-1009. The subgroup was Pbam and the lattice parameters were a= 5.424 Å, b= 10.23 Å, c= 3.735 Å. Hexagonal structured crystalline peaks were observed for $SrMnO_3$ and the lattice parameters were a= 5.44 Å ,c= 9.080 Å was matched with the JCPDS card no 24-1213. The average crystallite sizes of the synthesized samples were estimated from the major diffraction peaks using the Scherrer formula $D = K\lambda / \beta\cos\theta$, where K is constant (K = 0.94), λ is the wavelength (1.5418 Å), θ is the Bragg angle and β is full width half maximum (FWHM) that is, broadening due to the crystallite dimensions. The average crystallite size of the prepared CMO and SMO samples by hydrothermal method with and without citric acid were 41, 53 nm and 52, 61 nm respectively where citric acid as chelating agent controlled the size of the nanomaterials [17].

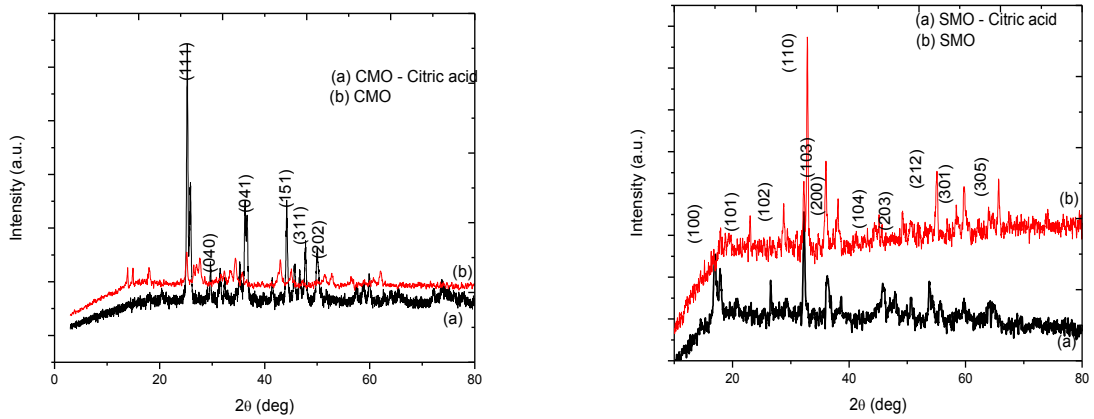

1(a) **1(b)**

Fig. 1. XRD Pattern of (a) CMO and (b) SMO nanomaterials

Fig 2(a, b) exhibits the surface morphology of CMO and SMO nanomaterials. The grains were agglomerated while homogeneously dispersed grains found in the samples where citric acid was used as chelating agent. The samples were in

porous nature where it was generated due to the evolution of carbon dioxide during the decomposition of doped manganese oxide nanoparticles. The prepared samples in the presence of citric acid were quite uniform and mono dispersed, whereas the samples prepared in the absence of chelating agent were agglomerated and poly dispersed. Randomly oriented grains were attained as expected for the typical structure of CMO and SMO nanomaterials and the average grain size was seemed to be in the range of a few nanometers as determined by using Scherrer formulae from X-ray diffraction analysis[18].

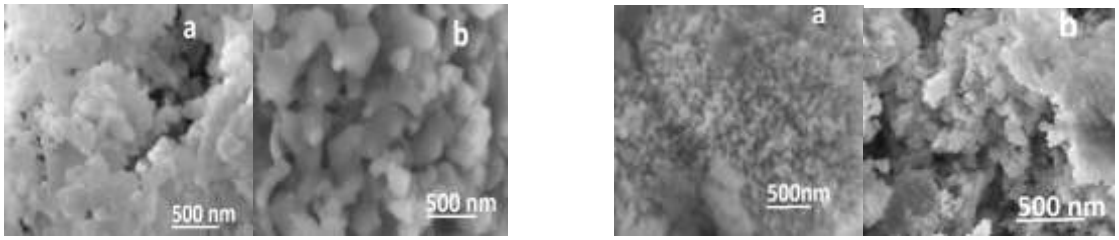

2(a) **2(b)**

Fig. 2. SEM Micrograph of (a) CMO and (b) SMO nanocrystals

The formation of CMO and SMO nanomaterials were further established by FTIR spectroscopy as shown in fig 3(a, b). The band around 3500 cm^{-1} corresponds to the O-H mode of vibration and the strong asymmetric stretching mode of vibration of C=O was scrutinized at around 1450 cm^{-1}. The symmetric stretching occurs at 850 cm^{-1} indicates the vibration of NO_3^{-1} ions and the standard peak of CMO and SMO nanocrystals was appeared in the region of 550 cm^{-1} [19].The sharp peaks have been observed for the samples prepared with citric acid as chelating agent.

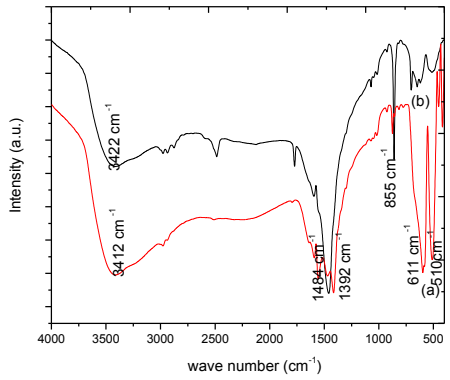

3(a)

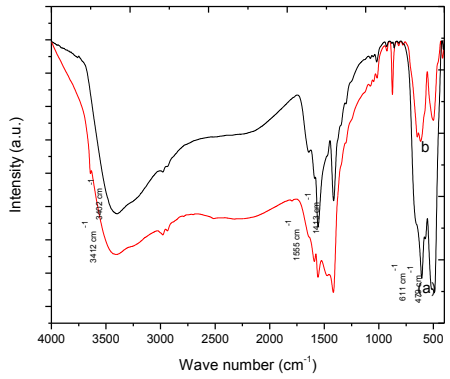

3(b)

Fig. 3. FTIR Spectra of (a) CMO Nanocrystals (b) SMO Nanocrystals

The optical properties of CMO and SMO nanocrystals were characterized by UV-vis spectroscopy as shown in fig.4 (a, b). The formation of CMO and SMO nanomaterials were indicated by the absorption peaks at 319,321 nm and 264, 292 nm. The band gap E_g was calculated from the equation $(\alpha h\nu)^n = B\ (h\nu - E_g)$, Where α is the absorption coefficient, hν is the photon energy, B is dimensional constant, and n is the index representing the transmission order, where n=2 for an direct band gap and n=1/2 for indirect band gap [20]. The band gap was determined by extrapolating the linear portion of the plot relating $(\alpha h\nu)^{1/2}$ versus hν to the value of α=0. The band gap of the prepared samples were 2.64, 2.51 eV and 2.91, 2.7 eV for CMO and SMO nanomaterials respectively. The higher band gap value could be ascribed to a smaller crystallite size of the nanomaterials [21].

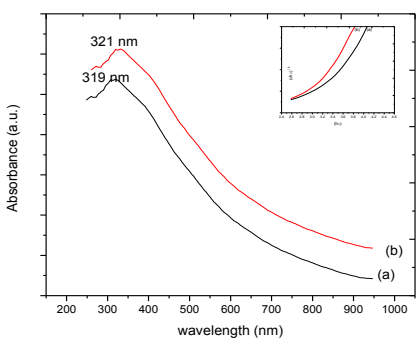

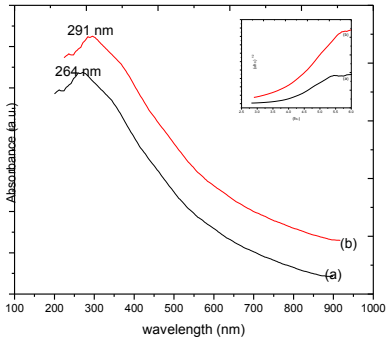

4(a) **4(b)**

Fig.4. UV – Visible Spectra of (a) CMO and (b) SMO Nanomaterials

4. Conclusion

CMO and SMO nanomaterials were synthesized by using hydrothermal method at pH 9.2 with and without citric acid as chelating agent. The XRD analysis confirmed that good crystalline material obtained for the sample prepared with citric acid. The addition of citric acid enhanced the crystallization process at low temperature and reduced the average crystallite size. SEM Micrograph showed a high degree of homogeneously dispersed and non agglomerated nanograins observed for the same sample. The formations of CMO and SMO nanomaterials have been signified by FTIR spectroscopy. From the absorption peak, band gap increased for the smaller crystallite size of the nanomaterials and it was found to be 2.64 eV and 2.91 eV for CMO and SMO nanomaterials. These results suggest that there might be the scope for improving n – type materials for high temperature thermoelectric applications.

References

1. M. A. Pena, J. L. G. Fierro, Chem. Rev., 101 , 1981 (2001)
2. R. Chiba, H. Orui, T. Komatsu, Y. Tabata, K. Nozawa, M. Arakawa, K. Sato, H. B. Arai, J. Electro chem. Soc., 155, 575 (2008)
3. L. Abdul Khalam, H. Sreemoolanathan, R. Ratheesh, P. Mohanan, M. T. Sebastian, Mater. Sci. Eng., 107,264 (2004)
4. J. Dho, W. S. Kim, E. O. Chi, N. H. Hur, S. H. Park, H. C. R , Solid State Commun., 125, 143 (2003)
5. G. Chen, M. S. Dresselhaus, D. Dresselhaus, J. P. Fleurial, T. Caillat, Int. Mater. Rev., 48, 45 (2003)
6. J. Pei, G. Chen, N. Zhou, D. Q. Lu, F. Q. Xiao, Physica B., 406, 571 (2011)
7. J. F. Nakahara, T. Takeshita, M. J. Tschetter, B. J. Beaudry, J. K. A. Gshneider, J. Appl. Phys., 63, 2331 (1998)
8. M. Yoshimura, S. E. Yoo, M. Hayashi, N. Ishizawa, J. Appl. Phys., 28, 2007 (1989)
9. S. Komarneni, S. Roy, Mater. Lett., 3,165 (1985)
10. Sridhar Komarneni , Young Dong Noh , Joo Young Kim , Seok Han Kim , Hiroaki Katsuki, Z. Naturforsch., 65b, 1033 (2010)
11. A. Pathak, P. Pramanik, Pinsa., 67, 47 (2001)
12. D. J. Anderton, F. R. Sale, Powder Metall., 22, 14 (1979).
13. M. S. G. Baythoun, F. R. Sale, J. Mater. Sci., 17, 2757 (1982).
14. Jianrong Niu, Jiguang Deng, Wei Liu, Lei Zhang, Guozhi Wang, Hongxing Dai, Hong He, Xuehong Zi, catal.Today., 126, 420 (2007)
15. R. Ma, K. Takada, K. Fukuda, N. Iyi, Y. Bando, T. Sasaki, Angew. Chem. Int. Ed., 47, 86 (2008)

16. Hohyun Lee, Daryoosh Vasahee, Wang DZ, Mildred S Dresselhaus, Ren ZF, Gang Chen, J.Appl. Phys., 107, 94308 (2010)
17. A. Shalaby, A. Bachvarova-Nedelcheva , R. Iordanova , Y. Dimitriev, J.Chem.Tech.Metay., 48, 585 (2013)
18. Provas Pal, Sandip K. Pahari, Arnab Kanti Giri, Sagar Pal, Hari C. Bajaj, Asit Baran Panda, J. Mater. Chem. A., 1, 10251 (2013)
19. R. Wahab, S. G. Ansari, H. K. Seo, Y. S. Kim, E. K. Suh, H. S. Shin, Solid State Sci., 11, 439 (2009)
20. R. Wahab, S. G. Ansari, Y. S. Kim, H. K. Seo, G. S. Kim, G. Khang, H. S. Shin, Mater. Res. Bull., 42, 1640 (2007)
21. X. M. Lu, J. S. Zhu, W. Y. Zhang, G. Q. Ma and Y. N. Wang, Thin Solid Films., 274, 165 (1996)

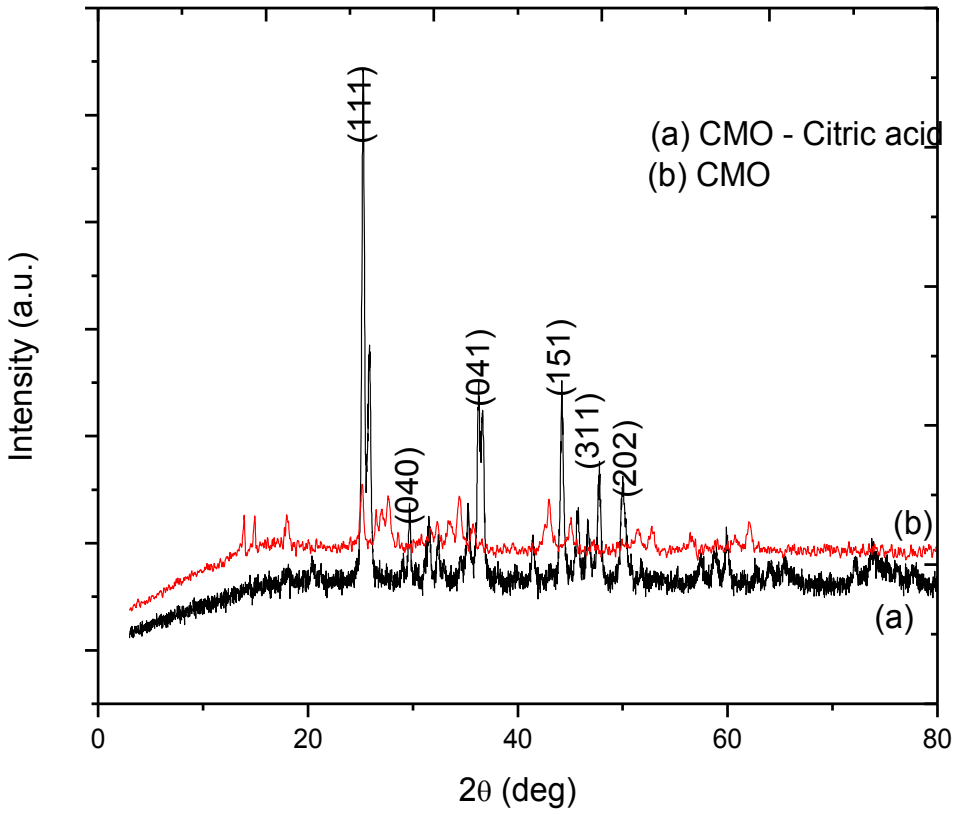

1(a)

Fig. 1. XRD Pattern of (a) CMO and (b) SMO nanomaterials

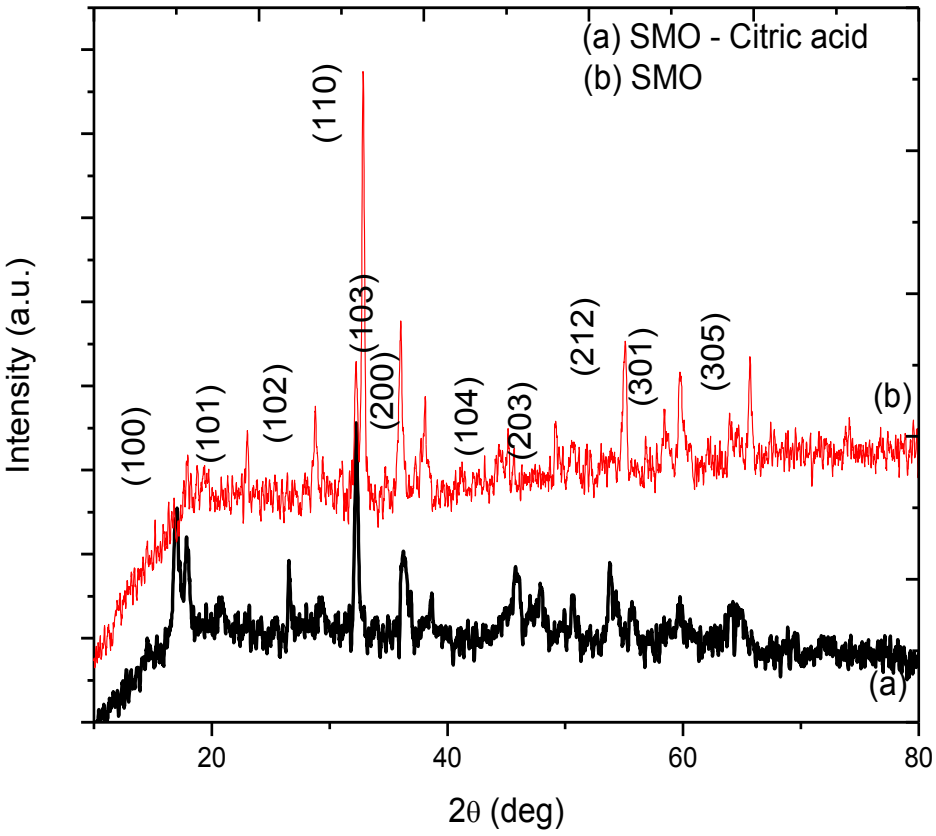

1(b)

Fig. 1. XRD Pattern of (a) CMO and (b) SMO nanomaterials

Hydrothermal Synthesis of Perovskite Oxides $CaMnO_3$ and $SrMnO_3$

S. Berbeth Mary[1], D.Edward Christy[2], S. Selvakumari[1], A. Leo Rajesh[1*]

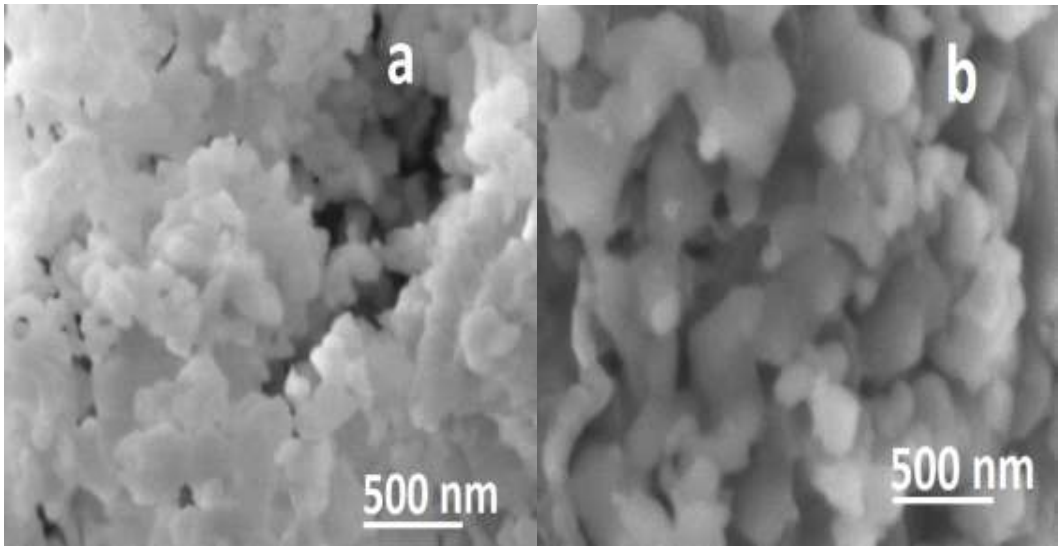

2(a)

Fig. 2. SEM Micrograph of (a) CMO and (b) SMO nanocrystals

Hydrothermal Synthesis of Perovskite Oxides $CaMnO_3$ and $SrMnO_3$
S. Berbeth Mary[1], D.Edward Christy[2], S. Selvakumari[1], A. Leo Rajesh[1*]

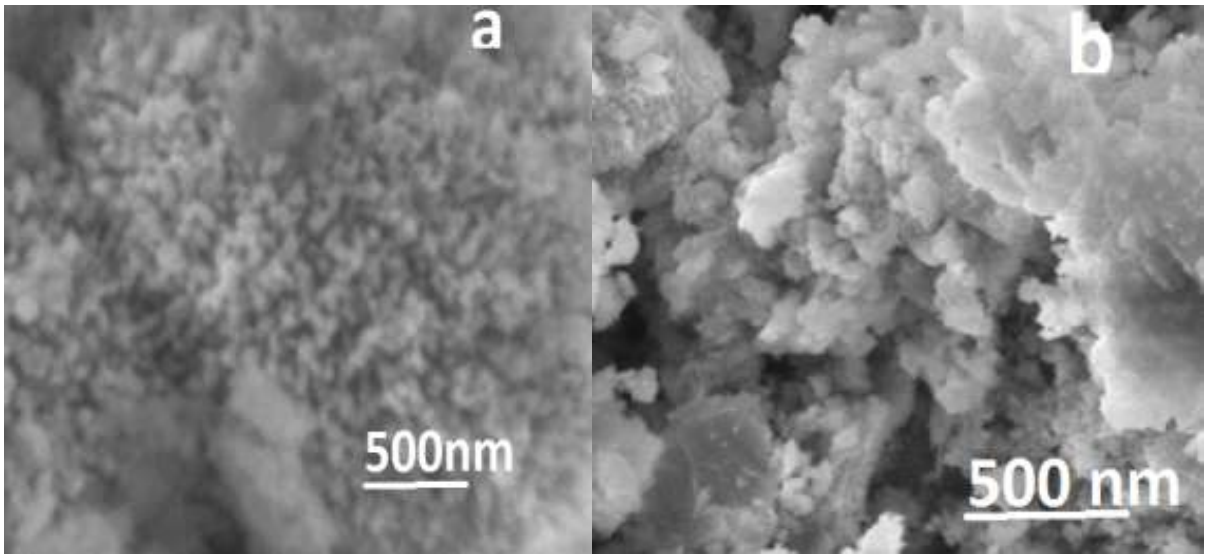

2(b)

Fig. 2. SEM Micrograph of (a) CMO and (b) SMO nanocrystals

Hydrothermal Synthesis of Perovskite Oxides $CaMnO_3$ and $SrMnO_3$
S. Berbeth Mary[1], D.Edward Christy[2], S. Selvakumari[1], A. Leo Rajesh[1*]

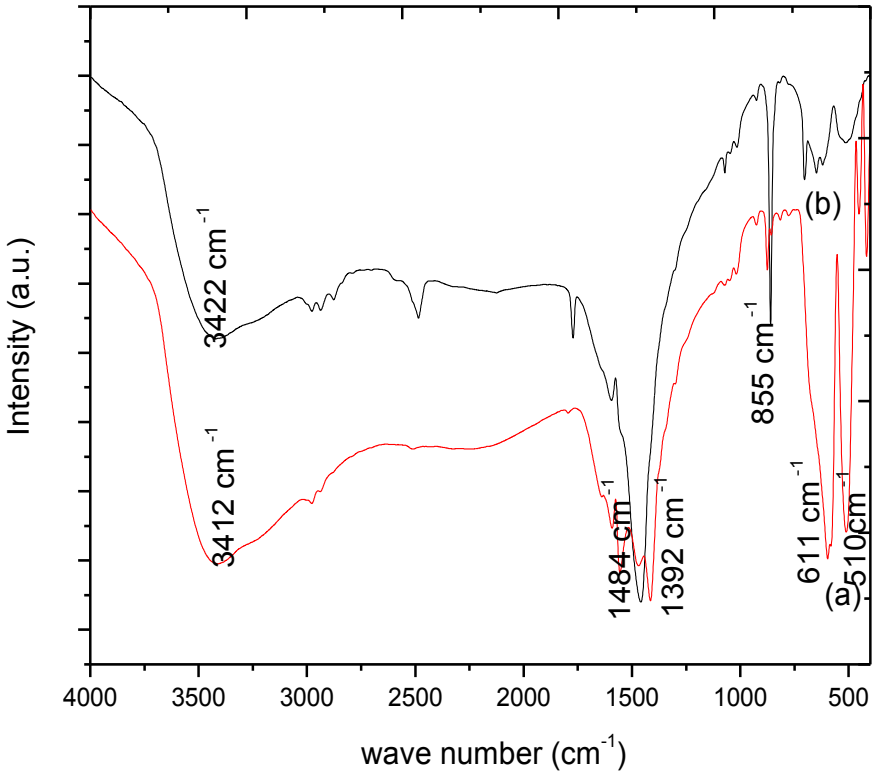

3(a)

Fig. 3. FTIR Spectra of (a) CMO Nanocrystals (b) SMO Nanocrystals

Hydrothermal Synthesis of Perovskite Oxides $CaMnO_3$ and $SrMnO_3$

S. Berbeth Mary[1], D.Edward Christy[2], S. Selvakumari[1], A. Leo Rajesh[1*]

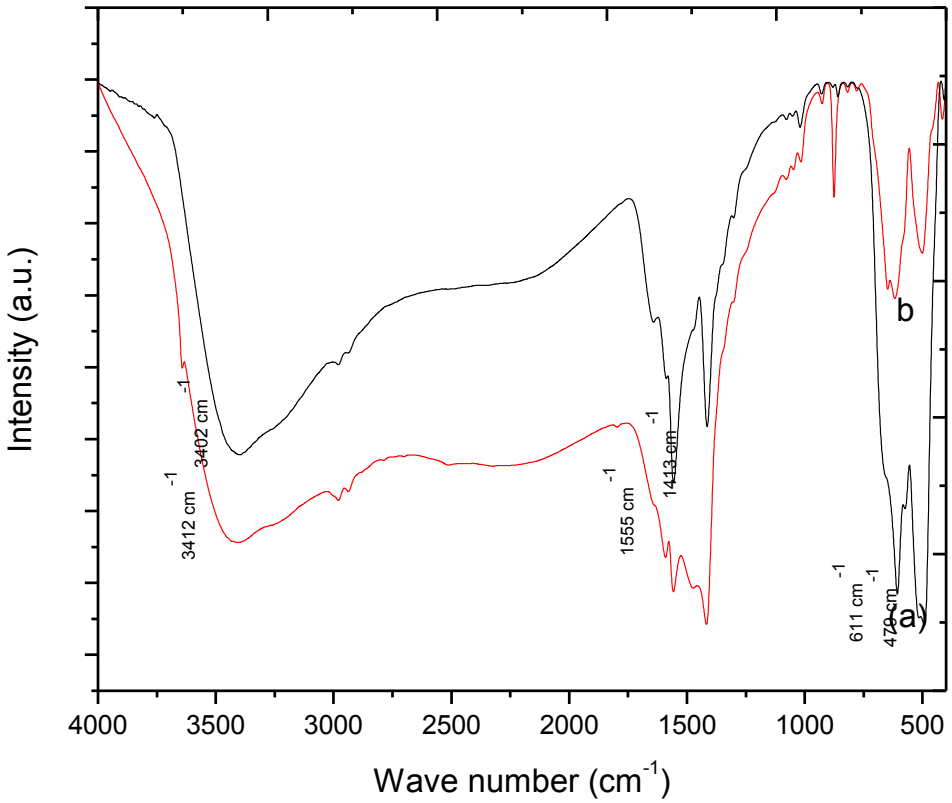

3(b)

Fig. 3. FTIR Spectra of (a) CMO Nanocrystals (b) SMO Nanocrystals

Hydrothermal Synthesis of Perovskite Oxides $CaMnO_3$ and $SrMnO_3$

S. Berbeth Mary[1], D.Edward Christy[2], S. Selvakumari[1], A. Leo Rajesh[1*]

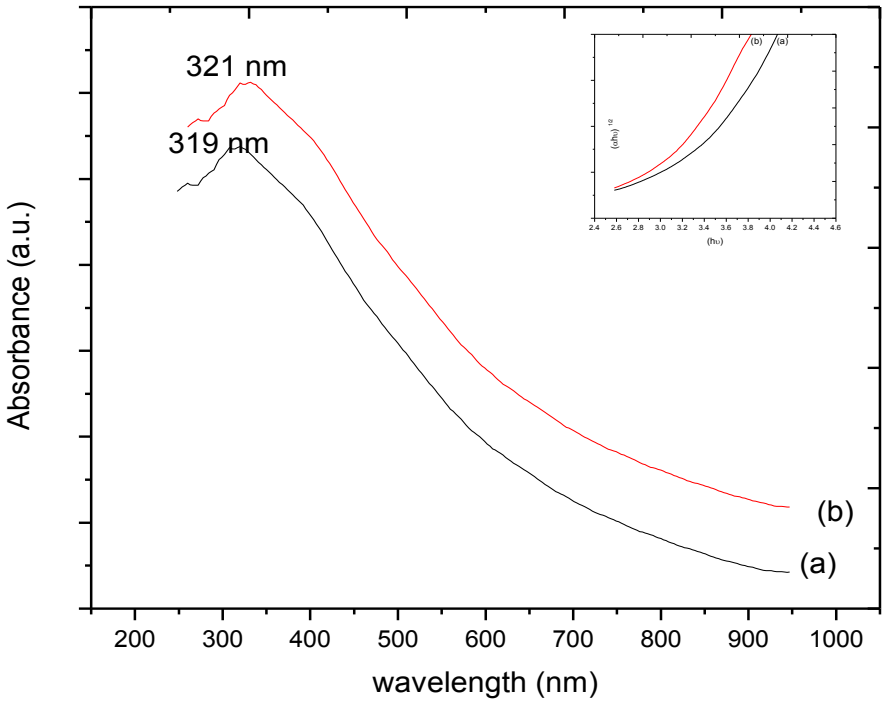

4(a)

Fig.4. UV – Visible Spectra of (a) CMO and (b) SMO Nanomaterials

Hydrothermal Synthesis of Perovskite Oxides $CaMnO_3$ and $SrMnO_3$
S. Berbeth Mary[1], D.Edward Christy[2], S. Selvakumari[1], A. Leo Rajesh[1*]

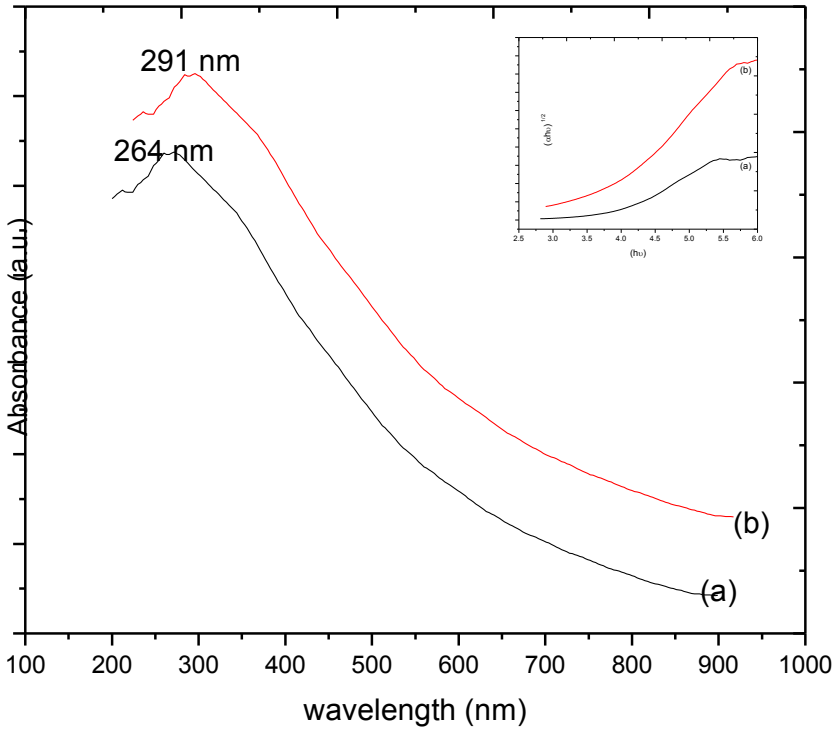

4(b)

Fig.4. UV – Visible Spectra of (a) CMO and (b) SMO Nanomaterials

Hydrothermal Synthesis of Perovskite Oxides $CaMnO_3$ and $SrMnO_3$

S. Berbeth Mary[1], D.Edward Christy[2], S. Selvakumari[1], A. Leo Rajesh[1*]

